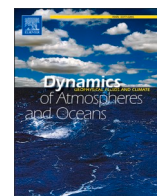


Contents lists available at [ScienceDirect](https://www.sciencedirect.com)

Dynamics of Atmospheres and Oceans

journal homepage: www.elsevier.com/locate/dynatmoce

Marine heatwaves intensification, expansion and departure into the permanent state over the Tropical Indian Ocean: A regional earth system model assessment

Pankaj Kumar^{a,*}, Anand Singh Dinesh^a, Alok Kumar Mishra^a,
Lokesh Kumar Pandey^a, Dmitry V. Sein^{b,c}, Vladimir A. Ryabchenko^b

^a Department of Earth and Environmental Sciences, Indian Institute of Science Education and Research Bhopal, Bhopal, India

^b Shirshov Institute of Oceanology, Russian Academy of Sciences, Moscow, Russia

^c Alfred Wegener Institute for Polar and Marine Research, Bremerhaven, Germany

ARTICLE INFO

Keywords:

Marine heatwave
Climate change
Extreme event
Regional Earth System Model
Future scenarios

ABSTRACT

This study employed a regional earth system model, namely ROM over the CORDEX-SA domain, to investigate the future changes in the Marine heatwaves (MHWs) with respect to the historical baseline period (1976–2005) in the three time-slices, explicitly, near future (NRF; 2010–2039), middle future (MDF; 2040–2069), and far future (FRF; 2070–2099) under two emission scenarios, Representative Concentration Pathway (RCP4.5 and RCP8.5). For the historical period, ROM showed a reasonable agreement with observed MHWs metrics and their trends and outperformed the forcing General Circulation Model and Multi-Model Ensemble of CMIP5 models. The future MHWs are expected to increase in intensity and duration. The continuous lengthening of MHWs duration leads to a permanent MHW state condition with strong spatial variability in its appearance. The first permanent MHW will emerge in both RCPs, while the absolute permanent MHW state is mainly visible in RCP8.5. The genesis and augmentation in the MHWs intensity is associated with local air-sea fluxes, however, in the long term, the increase in the mean SST in the future led to the rise of MHWs activity. The diagnosis of El Niño Southern Oscillation teleconnection and Indian Ocean Dipole on the MHWs is investigated. During the El Niño regime, not only did the proportion of the Tropical Indian Ocean experiencing MHWs increase but also an increase in the intensity is evident. IOD controls the MHWs metrics in the proximity of the western box and eastern box during its positive and negative phases.

1. Introduction

The global ocean has been getting warmer in recent decades and is expected to continue to warm in the future (Alexander et al., 2018). As a result, the discrete and prolonged events of anomalously warm water known as Marine heatwaves (MHWs) (Hobday et al., 2016) have arisen not only on the marginal seas or coastal regions but also on the open ocean globally. Various studies have reported unprecedented MHW events over different parts of the global ocean, such as the Western Australia MHWs in 2011 (Pearce and Feng,

* Correspondence to: Department of Earth and Environmental Sciences, Indian Institute of Science Education and Research Bhopal, Bhopal 462066, India.

E-mail address: kumarp@iiserb.ac.in (P. Kumar).

<https://doi.org/10.1016/j.dynatmoce.2023.101408>

Received 10 May 2023; Received in revised form 1 November 2023; Accepted 2 November 2023

Available online 7 November 2023

0377-0265/© 2023 Elsevier B.V. All rights reserved.

2013), the northwest Atlantic MHWs in 2012 (Chen et al., 2014), Ningaloo Niño in the eastern Indian Ocean during 2012 (Kataoka et al., 2014; Feng et al., 2015; Marshall et al., 2015), the 2012 and 2015 Mediterranean Sea MHWs (Darmaraki et al., 2019), the 2013/14 western South Atlantic MHWs (Rodrigues et al., 2019), the persistent 2014–2016 “Blob” in the North Pacific (Bond et al., 2015; Di Lorenzo and Mantua, 2016), the 2015/16 MHWs spanning the southeastern Tropical Indian Ocean (TIO) to the Coral Sea (Benthuisen et al., 2020) and the 2017 southwestern Atlantic MHWs (Manta et al., 2018). Distinctly, these events have momentous ecological, social, and economic impacts. The onset of MHWs is attributable to the regional ocean and atmospheric processes such as ocean advection, air-sea fluxes, thermocline stability, wind stress and large-scale climate variability by teleconnection (Holbrook et al., 2019).

In the warming scenario of changing climate, a consistent increase in the frequency, intensity, and duration of MHWs, along with their repercussions on the marine ecosystem, has been witnessed (Oliver et al., 2019). The ongoing intensification of MHWs induces severe threats to the marine ecosystem and imposes devastating and long-lasting biological impacts. Marine species are reciprocating this thermal stress by the act of habitat relocation, shrinking ecosystem services, and mass mortality. The adverse effect of MHWs on the marine ecosystem is observed predominantly as coral bleaching (Le Nohaïc et al., 2017), loss of kelp marine forests, sea star wasting disease (Bates et al., 2009), toxic algal blooms (McCabe et al., 2016), mortality of benthic communities (Garrabou et al., 2009), fisheries sector (Feng et al., 2013). Furthermore, MHWs influence the marine food industry by depressing environmental suitability for economically important fisheries and aquaculture, leading to the increased risk of food security, economic loss, and people's livelihoods globally. These facts necessitate improving the understanding of MHWs-prompted changes that will be crucial for the future management of ocean and coastal resources and the development of new strategies for managing coastal areas and fisheries.

An effort has been made to understand the extreme temperature events variability and trend over the Pacific and Atlantic oceans and their associated drivers (Chen et al., 2014; Holbrook et al., 2022; Hu et al., 2021). However, the Tropical Indian Ocean (TIO) which is warming at an alarming rate (Gnanaseelan et al., 2017), has received less attention in the context of MHWs and associated dynamics. The available studies on TIO focus on the diagnosis of MHWs characteristics in the Arabian Sea and impacts of climate modes (Indian Ocean Dipole; IOD and El Niño Southern Oscillation; ENSO) on the MHWs (Chatterjee et al., 2022), genesis and trends of MHWs and how they influence the Indian summer monsoon rainfall (Saranya et al., 2022), the interaction of MHWs with Tropical Cyclones (Rathore et al., 2022), the impact of MHWs on biogeochemistry such as chlorophyll, oxygen, net primary productivity, nitrate, phosphate and silicate etc. (Chakraborty et al., 2023). Further Holbrook et al. (2019) shows that over majority of TIO, the ENSO and IOD has greatest significant impact on enhancing or suppressing the number of MHWs days. In another study Sen Gupta et al. (2020) has shown the drivers of most extremes MHWs on global scale including TIO.

The TIO is distinctive as Asian countries surround it from the north, and the resulting land-sea temperature gradient gives rise to one of the greatest summer monsoons on the earth. The Northern TIO shows large marine primary productivity during the South Asian summer monsoon (Roxy et al., 2016, Sein et al., 2022). The Northern TIO variability influences and gets influenced by Indian Summer Monsoon variability (M. Roxy et al., 2012; M. Roxy & Tanimoto, 2007; Singh and Dasgupta, 2017; Srivastava et al., 2018). Moreover, the TIO has active air-sea interactions over a variety of timescales. Various studies have explored the TIO characteristics using standalone ocean models (Pandey et al., 2021; Pandey and Dwivedi, 2021; Srivastava et al., 2016; Suneet et al., 2019). The standalone ocean models are a good tool to provide insights, but it has some limitations for correct state estimation due to the lack of air-sea interaction without atmospheric coupling. The study by Di Sante et al. (2019), Kumar et al. (2014a), Kumar et al. (2014b), Mishra et al. (2021) and Sein et al. (2020) shows the advantage of the coupled model over the standalone ocean model for apprehending ocean state.

To better understand ocean-atmosphere interaction, coupled ocean-atmosphere general circulation models are frequently used. Recent MHW studies based on these coupled general circulation models suggested future increases in the severity and duration of MHW events (Frölicher et al., 2018, Oliver et al., 2019; Plecha & Soares, 2020). However, these findings are based on coarse-resolution climate models with limitations in resolving fine-scale features and coastal processes (Giorgi and Gao, 2018; Mishra et al. 2023). On the other hand, the regional earth system model (RESM) systematically resolves the small-scale processes and their interaction among the different simulated components of the earth system. A number of the studies have highlighted the importance of the RESM and its reliability in projected fields, especially for the extremes on a regional scale (Darmaraki et al., 2019; Kumar et al., 2014a; Kumar et al., 2014b; Kumar et al., 2023; Sein et al., 2020; Zhu, Remedio et al., 2020). Additionally, in the Med-CORDEX initiative, an ensemble of fully-coupled RESMs was utilized for studying the evolution of future MHWs over the Mediterranean Sea, a substantial spread in projected MHWs intensity and duration with the highest (lowest) change in RCP8.5 (RCP2.6) were observed (Darmaraki et al., 2019). The novelty of this manuscript is that, for the first time, this study uses the Regional Earth System Model (RESM), namely ROM, to understand the future MHWs over the CORDEX-South Asia domain. ROM is not only a high-resolution but also a fully coupled Regional Earth System Model with a better representation of the physical and dynamical processes of earth system components, i.e., atmosphere, ocean, and hydrological components along with the full biogeochemical cycles that gives a better representation to suitably simulate the regional climate in comparison with Earth System Models and standalone Regional Climate Models (RCM). ROM shows the potential over CMIP5/CMIP6 and their ensemble for various aspects covering extreme weather and climate, atmosphere and ocean characteristics as well as the Indian monsoon, which has been reported in previous studies on a broader scale (Kumar et al., 2014a; Kumar et al., 2014b; Kumar et al., 2022; Mishra et al., 2021; Dubey et al., 2021; Saharwardi et al., 2021; Kumari and Kumar, 2023, Sein et al., 2022).

Therefore, this study employed a RESM, namely ROM, with a varying horizontal resolution of the ocean model, ~5 km over coastal regions and ~48 km over the open TIO, to quantify MHWs variability in recent decades and its future evolution under two emissions scenarios RCP4.5 and RCP8.5. To the author's best knowledge, there has been a limited study focusing on the future changes in the MHW's characteristics over the TIO using RESM.

2. Material and methods

2.1. Model description and components

This study uses a RESM, namely ROM (Sein et al., 2015, 2020, 2022) that consists of (i) The regional climate model (REMO) (Jacob, 2001; Jacob & Podzun, 1997) as an atmospheric component and (ii) global Max Planck Institute Ocean Model (MPIOM) (Jungclaus et al., 2013) as ocean component. (iii) global Hydrological Discharge model (HD) (Hagemann and Dümenil, 1998), (iv) ocean biogeochemistry model Hamburg Ocean Carbon Cycle (HAMOCC) (Maier-Reimer et al., 2005). The mentioned models were integrated using the Ocean-Atmosphere Sea Ice Soil Version 3 (OASIS 3) coupler from the European Centre for Research and Advanced Training in Scientific Computation (Sein et al., 2015; Sein et al., 2022; Zhu et al., 2020), Fig. 1. During the processing of the OASIS coupler at each coupling time step, i.e. every 3 h in our study, the REMO receives its lower boundary conditions over the sea and sea ice surfaces from the MPIOM ocean model and allocates heat, atmospheric momentum, and water fluxes to the MPIOM (Sein et al., 2015; Zhu et al., 2020). Note, that all the model components of ROM, except REMO are global. Further details about the model integration and detailed dynamics can be obtained from Kumar et al. (2022), Mishra et al. (2021), Sein et al. (2015) and Sein et al. (2022).

After ca. 100 years of spin-up, three simulations were carried out at a horizontal resolution of $0.44^\circ \times 0.44^\circ$ using the global coupled model MPI-ESM-LR (hereafter ESM) data as lateral boundary conditions for REMO and as atmospheric forcing for MPIOM outside the coupled area. The first simulation was for the historical period 1950–2005, the second and third simulation was for the future projections covering 2006–2099 using the RCP 4.5 and RCP 8.5 emission scenarios. The output of future simulation for each scenario was categorized into three different time slices for deriving MHW characteristics with respect to the historical baseline period (1976–2005). The future period was classified as (i) near future (NRF; 2010–2039) (ii) middle-future (MDF; 2040–2069) (iii) far future (FRF; 2070–2099). The sea surface temperature (SST) and its extremes (MHW) from the model are validated from 1982 to 2005. In this study, this period is called as an evaluation period. The evaluation period is a subset of the historical period and it is specifically selected, which overlaps with the availability of National Oceanic and Atmospheric Administration (NOAA) Optimum Interpolation Sea Surface Temperature (OISST) datasets (available from 1982 onwards) with which the model performance has been evaluated. Therefore, for evaluation, all ROM data were interpolated to the OISST grids.

2.2. Observational Datasets

This study uses daily SST data at $1/4^\circ$ from the NOAA OISST v2.0 (Reynolds et al., 2007) to examine the model performance in capturing MHW over the evaluation period (1982–2005). This data incorporates observations from platforms such as Advanced very high-Resolution Radiometer satellite retrievals, ships, buoys, and Argo floats on a regular global grid.

2.3. MHW Estimation

MHWs were identified at each grid cell by calculating the time series of SST anomalies relative to the 30-year climatological SST. A MHW is declared when the local SST exceeds the seasonally varying threshold, i.e. 90th percentile, for five or more days (Hobday et al., 2016; Hobday et al., 2018; Schaeffer & Roughan, 2017). Selecting a threshold for detecting MHW is a crucial decision because this

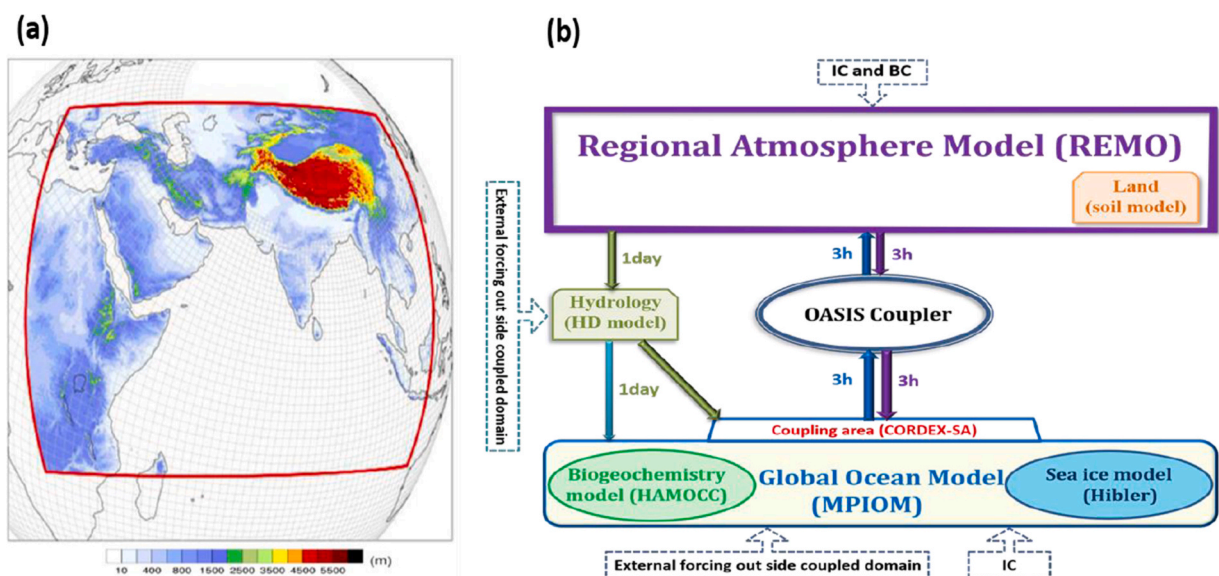


Fig. 1. Model domain and component.

alters the number of detected MHWs methodically. This study prefers the seasonally varying percentiles method over the fixed threshold method since the fixed threshold fluctuates significantly by region for large analysis (Hobday et al., 2018). The seasonally varying threshold has been determined from a long-term fixed baseline period of historical data, i.e., 1976–2005 which was further used to calculate MHW metrics in all-time slices, i.e., NRF, MDF, and FRF. The selection of a fixed baseline period for MHW projection analysis is persistent with the previously reported studies (Frölicher et al., 2018; Oliver et al., 2019) which demonstrate the future changes with respect to the historical climate.

During analysis, the daily climatology and threshold were computed by incorporating daily SST within 11-day windows with smoothing using a 31-day moving average. Additionally, a break of fewer than 2 days between the events is considered a single event. Finally, a set of MHW metrics were considered, namely, the number of MHW events, maximum intensity (maximum temperature anomaly during an event), annual duration of MHW (number of MHW days in a year) and categories (Moderate, Strong, Severe and Extreme) of MHW. The MHW categories were defined based on the degree to which SST exceeds the climatology. The MHW category is determined by using the formula from Hobday et al. (2018) which is as below.

$$MHW \text{ Category} = \frac{SST - SST_{clim}}{SST_{90percentile} - SST_{clim}} \quad (1)$$

Hence, the MHW can be categorized as moderate ($1 \leq MHW \text{ Category} < 2$), strong ($2 \leq MHW \text{ Category} < 3$), severe ($3 \leq MHW \text{ Category} < 4$), and extreme ($4 \leq MHW \text{ Category}$).

2.4. Permanent MHW state

This study follows the definitions used in the study by Oliver et al. (2019) to determine the permanent MHW state. A permanent MHW state simply means that SST exceeds the threshold values continuously and yields MHWs-like conditions for 365 days. Following this, the first permanent MHW (the foremost year in which MHWs duration will be 365 days) and absolute permanent MHW (the year after which permanent MHW condition will prevail throughout the upcoming years) over each grid of the model domain are computed.

As the name suggests, the first permanent MHW state is the time when the SST exceeded the 90th percentile threshold for the very first time for 365 days. For example, for any random location let's consider the year 2040 to be the first permanent MHW and it is not mandatory for the region to undergo into MHW conditions for the same duration (365 days) in the subsequent years. An implication of this is that the marine ecosystem will be exposed to 365 days of MHWs in the year 2040 and then followed by a subsequent perceptible temperature relief, facilitating the recovery of marine organisms in the coming years.

But what if after experiencing 365 MHWs days in any specific year, each incoming year is a like MHWs condition only, which does not allow the marine ecosystem to settle. To address this particular case, we investigate the absolute permanent MHW state. Thus, we look for a date after which every incoming year will witness MHWs lasting precisely 365 days. This will pinpoint specific ocean areas where softening of the MHW's impact will be more required. This information can be leveraged to improve the planning of local response and can be relevant in various ecological studies also it will be used to buy more time for species and ecosystems to adjust and transform.

2.5. Atmospheric parameters and mixed layer heat budget

The atmospheric parameters such as wind speed (WS) at 850 hPa, surface shortwave radiation (SWR), surface longwave radiation (LWR), surface sensible heat flux (SHF), and surface latent heat flux (LHF) are key modulators of ocean characteristics, including the surface and subsurface temperature (Srivastava et al., 2016). These atmospheric parameters have positive and negative feedback on SST and hence modulate MHWs. In the undisturbed natural oceanic system, solar radiation, in conjunction with oceanic processes, is the primary source of ocean heating over the region. Temporally MHWs are a synoptic phenomenon (days to weeks), therefore, analyzing the role of these atmospheric parameters during MHW events will be critical. Hence daily data of these atmospheric parameters are utilized.

As the SST is dependent on the various physical processes that take place at the sea surface and in the mixed layer. Therefore, the role of local parameters in increasing the SST has been investigated using mixed layer heat budget analysis, computed from 1976 to 2099 using monthly data (due to availability of u, v, w current on the monthly scale). Notably, here the temporal resolution of mixed heat budget terms is at a monthly scale and therefore, investigating the role of monthly heat budget terms on the MHWs is not feasible here as MHWs are a phenomenon that lasts from days to weeks. However, these terms demonstrate their influence on the augmentation/reduction of the surface temperature from historical to future periods.

Mathematically the processes in the mixed layer heat budget are represented as Eq. 2 (Vialard et al., 2001; Vialard and Delecluse, 1998).

$$\frac{1}{\tau} \delta T_{ml} = -\frac{1}{h} \int_{-h}^0 u \partial_x T dz - \frac{1}{h} \int_{-h}^0 v \partial_y T dz - \frac{1}{h} \int_{-h}^0 D1(T) dz - \frac{1}{h} (T_{ml} - T_{-h})(w_{-h} + \partial_t h) - \frac{1}{h} [k_z \partial_z T]_{-h} + \frac{Q_s(1 - F_{-h}) + Q_{ns}}{\rho_o C_p h} \quad (2)$$

where δT_{ml} is the increment of T_{ml} over a time interval (step) τ . The first and second term on the right-hand side is zonal and meridional temperature advection. The third and fourth term is the lateral mixing process and the vertical exchange of heat between the mixed layer and subsurface ocean, including upwelling $w_{-h}(T_{-h} - T_{ml})$, entrainment $\partial_t h(T_{-h} - T_{ml})$ and turbulent mixing at the bottom of the mixed layer $k_z \partial_z T_{-h}$. The last term on the right-hand side is atmospheric heat flux forcing. The “T” denotes the temperature, and “h” in

the equation is a time-varying model mixed layer depth. In the lateral mixing process, $D1(T)$ is the diffusion operator and this heat budget does not enumerate diffusion components because of their negligible contribution. “ K_z ” is a vertical mixing coefficient for the tracer. Q_s and Q_{ns} are solar and non-solar components of surface heat flux. F_h is part of the solar radiation Q_s that penetrate to depth h . ρ_o and C_p are seawater reference density and volumic heat capacity. All the estimated heat budget components have been converted to the same unit as ($^{\circ}C/day$).

2.6. Climate modes

The study of MHW contemplates various climate indices, as SST variability at the interannual scale over TIO has a robust correlation with the Indian Ocean Dipole (IOD) and El Niño Southern Oscillation (ENSO). A study by [Holbrook et al. \(2019\)](#) suggests that ENSO and IOD significantly impact the MHW events over most of the TIO region. Consequently, the Oceanic Niño Index (ONI) mode, defined as SST anomalies across (5 N-5S,170–120 W) with a 3-month running mean, relative to the base period of 1976–2005, has been calculated. When anomalies exceed $\pm 0.5^{\circ}C$ for five successive months, the El Niño or La Niña is declared ([Glantz and Ramirez, 2020](#); [NOAA., 2022](#); [Van Viet, 2021](#)). On the other hand, the monthly dipole mode index (DMI), which represents the IOD, is computed as the difference in SST between the west box ($10^{\circ}S-10^{\circ}N,50-70^{\circ}E$) and east box ($10^{\circ}S-0^{\circ}N,90-110^{\circ}E$). The running average of 3 months has been taken for the DMI index to smooth the time series. Positive (Negative) IOD events occur when the DMI exceeds (falls) $0.4^{\circ}C$ ($-0.4^{\circ}C$) for at least three months.

3. Results and discussion

3.1. Model evaluation

The reliability of the projected fields relies on the model’s potential to simulate the present climate. Therefore, it is worthwhile to examine the ability of the ROM to represent the salient ocean features. We have compared the mean annual SST during the evaluation period covering 24 years, 1982–2005 ([Fig. 2](#)). The figure shows that ROM resembles the observation in simulating the spatial distribution and correctly distinguishes low and high SST regions with some systematic biases ([Fig. 2a, b](#)). The bias map ([Fig. 2c](#)) shows that the biases over most parts of the TIO are negative. The positive bias is evident only over the western TIO, possibly due to reduced upwelling over the region, as reported in the earlier study ([Mishra et al., 2021](#)). Notably, over most TIO, the bias is less than the standard deviation (SD) ([Fig. 2d](#)) of corresponding regions. However, the bias over the eastern equatorial TIO region is slightly higher than the SD of observation. Additionally, the bias present over a patch of the latitudinal region of $\sim 10^{\circ}-20^{\circ}S$ (-1.5° to $-2.5^{\circ}C$) is slightly more than the SD of observation (1° to $2^{\circ}C$). The SD of observation and ROM are shown in [Fig. 2d](#) and (e). It can be easily perceived that ROM has good analogies with the observation in representing the SD. This strengthens the confidence in the reliability of projected fields using this model setup.

The MHWs characteristics are reported as a more robust metric that explains a stronger relationship with marine organisms than the mean and maximum SST ([Hayashida et al., 2020](#); [Smale et al., 2019](#)). Thus, it is worth diagnosing the ROM potential in

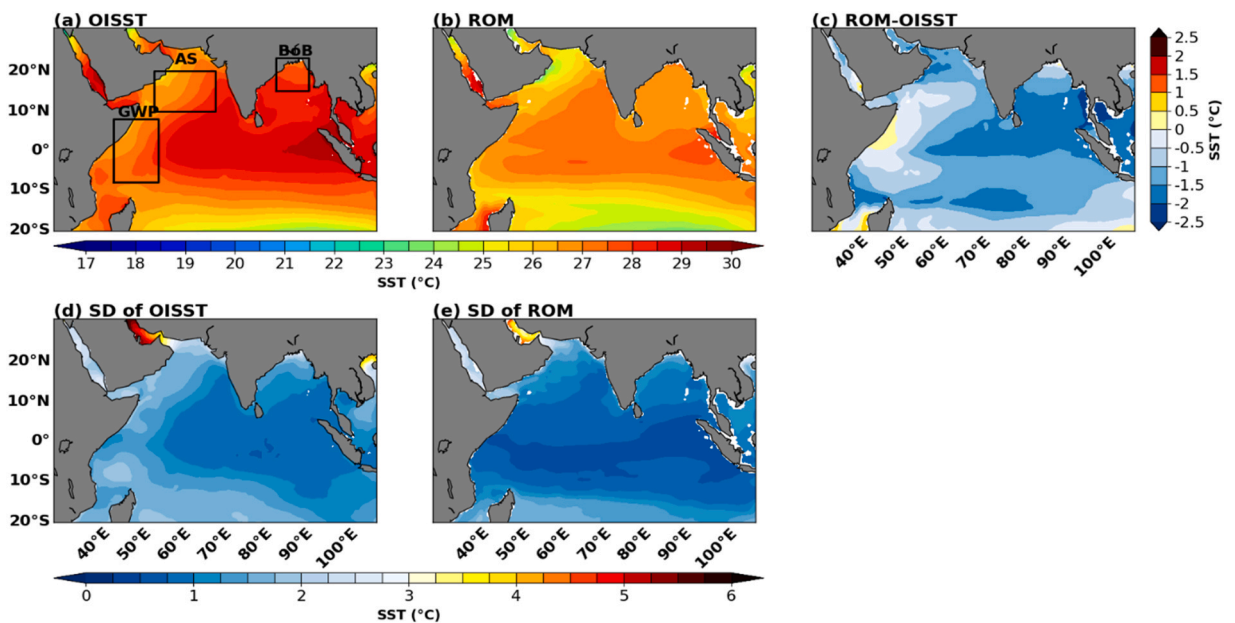


Fig. 2. Annual mean SST for the evaluation period (1982–2005) using (a) OISST and (b) ROM. (c) Bias (ROM-OISST) of mean SST (d) Standard Deviation of SST in OISST and (e) ROM.

reproducing these metrics. Additionally, in Fig. 3 the MHWs metrics obtained from ROM, its forcing model ESM and multimodal ensemble mean (MME) of the four best CMIP5 models (MPI-ESM-LR, NorESM1-M, CMCC-CMS, FGOALS-s2), that demonstrate better warming trends over Indian ocean (LI, J., & SU, J. (2020)) have been compared with the observed MHWs.

MHW events show substantial variability in observation data (Fig. 3(i)(a)). The eastern TIO shows more events than the western TIO, with some regional variation. As a result, the Bay of Bengal (BoB; 85–93°E 15–23°N) shows a greater number of events than the Arabian Sea (AS; 55–70°E 10–20°N). Noticeable variability is observed in the intensity (Fig. 3(i)(e)). The observed spatial patterns of maximum MHW intensity are characterized by more intense MHW along the north-western coast of AS, the Great Whirlpool (GWP; 45–56°E 8°S–8°N) region, and patches of northern BoB. The more extended MHWs duration has been centered around BoB, eastern AS, and latitudinal regions of ~20°S (Fig. 3(i)(i)).

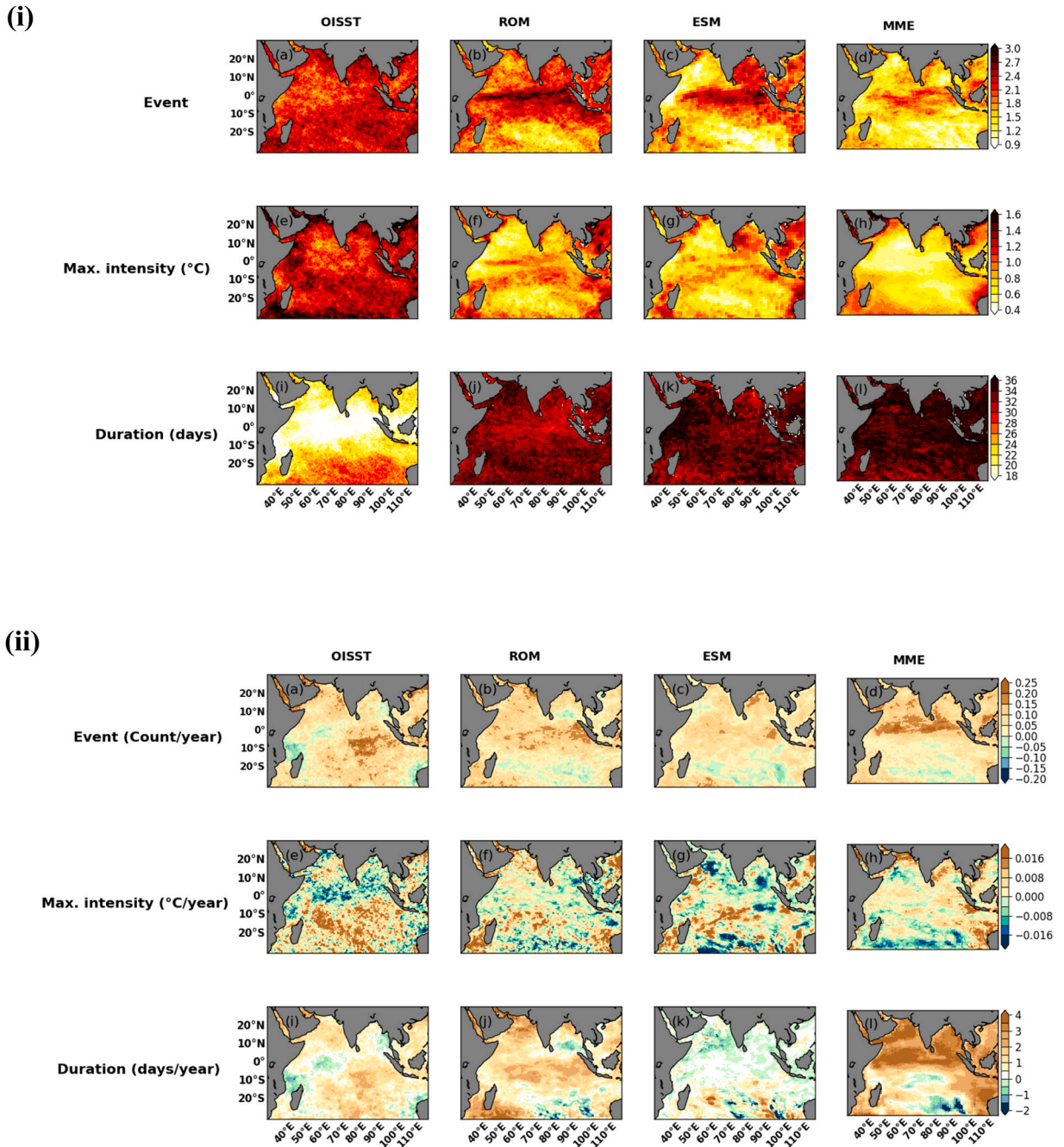


Fig. 3. (i) MHWs event, intensity and duration in observation and in the ROM, ESM and MME. (ii) Trend in MHWs event, intensity and duration for observation ROM, ESM and MME.

In comparison, both ROM and ESM overestimate the MHWs events centered around equatorial regions. While over the rest of TIO ROM, ESM and MME underestimate the events (Fig. 3(i)(b-d)) however over AS and southern TIO, ROM has a relatively lesser bias than the ESM and MME. All models underestimate the MHWs intensity primarily all over the TIO with varying magnitude (Fig. 3(i)(f-h)). Unlike the events and maximum intensity, all models overestimate the duration of the MHWs, indicating their tendency to produce prolonged events (Fig. 3(i)(j-l)). However, ROM has a relatively lesser bias than ESM and MME.

To make results more perspective, MHW characteristics from ROM ESM and MME are further discussed in terms of statistics-based indices against observation, i.e., root mean square error (RMSE), pattern correlation coefficient (CC) and skill score (SS) summarized in Table 1a. The ratio of RMSE of the model and SD of observation is considered as a skill score that has previously been used in the study by Dwivedi et al. (2017), Srivastava et al. (2016), Srivastava et al. (2018), Suneet et al. (2019). Values of skill scores less than one demonstrate the excellent skill of the model. ROM is performing well and has a higher correlation with observations than the ESM and MME for all the MHW metrics (Table 1a). In addition, the RMSE in ROM is less than the ESM and MME for all the metrics. Consequently, the skill score is less than one, which demonstrates the quality of ROM simulation. Therefore, it can be inferred from (Table 1a) that the ROM is comparatively better than the ESM and MME for simulating MHW metrics.

The model's tendency to produce similar trends, much like observation during the historical period, is also crucial in assessing the model's potential for future projection. Fig. 3(ii) shows that all models exhibit an analogous trend for the event in the northern TIO. The spatial variability of the intensity trend is captured reasonably well by all models, with slight regional variations in terms of magnitude. ROM over most of TIO has demonstrated a similar trend for the duration when compared against observation, though its magnitude is slightly higher. In contrast, ESM has a decreasing duration trend centered over AS and western BOB while MME shows a larger positive trend.

Based on the spatial patterns and statistics-based indices, ROM performs relatively better than the forcing model ESM and MME. Overall, ROM has shown satisfactory performance when compared to the observation in capturing the present climate SST and MHW, therefore, the future projection of MHW with this model will be interesting to address.

3.2. Projected changes in MHWs characteristics

The projected changes in the MHWs characteristics (future minus historical) are estimated under the two-emission scenarios, RCP4.5 and RCP8.5, covering 2006–2100. The results from both scenarios are discussed for three-time slices (i) near future (NRF;2010–2039) (ii) middle-future (MDF;2040–2069) (iii) far future (FRF; 2070–2099). Fig. 4(i)(a) and 4(ii)(a) represent that the MHW events are increasing during NRF over the entire TIO in both scenarios, however, magnitudes and spatial extents are highly dependent on the pathways of emissions scenarios, having slight larger signal in RCP8.5. In both RCPs, more pronounced changes (increment of 4–5 events/year) are noticed along with the western BoB, eastern coast around Sumatra and the equatorial region. Interestingly in both RCPs, MHW events in MDF (Fig. 4(i)(b) and 4(ii)(b)) are substantially lesser (3–5 times drop) than NRF, indicating the decline of the MHW frequency. This pattern of decline is followed up to the end of the 21st century. Some regions of maximum increase during NRF became the region of maximum decline (~2 events per year) in FRF (Fig. 4(i)(c) and 4(ii)(c)), for example, the equatorial and Sumatra regions. The rate and spatial extent of the decline are considerably higher in the RCP8.5 scenario than in the RCP4.5.

In the historical period, it was less likely for daily SST to climb above the 90th percentile threshold value which was derived from the fixed historical baseline period and hence only a few episodic MHW events were seen within a year. However, due to the consistent warming in the future, the future's daily SST will be higher than the 90th percentile threshold value based on the fixed historical baseline period; this enhanced SST will become a new normal in MDF and FRF periods. Therefore, MDF's and FRF's daily SST will easily exceed the 90th percentile threshold value leading to MHW-like conditions all around the year. In other words, a single MHW will exist for the entire year because future daily SST will be above the threshold for the entire year. For example, a location experiences five discrete MHW events in a year during the historical time, but the same location will now experience one MHW event in a year during the FRF (as in the future SST will always be above to the historical threshold value, hence event will start from 1 January and end at 31 December). Therefore, in the FRF, a drop of 4 events has been witnessed as a single MHW which covered all days of the year. This decline in MHW events might be spurious and mainly attributed to the current definition of the MHW, which is, the use of the fixed baseline period. There is still an ongoing debate on the utilization of fixed versus varying baseline periods for defining 90th percentile thresholds. The utilization of a fixed baseline period leads to some artificial MHWs metrics in the future as it does not take into account the warming of the oceans over time. However, considering the varying baseline periods will have no potential ecological significance, as highlighted by the research article Oliver et al. (2021) and Amaya et al. (2023). Currently, the majority of studies have opted fixed threshold in projecting the MHWs (Frölicher et al. 2018; Oliver et al. 2019; Darmaraki et al., 2019; Plecha & Soares, 2020) as it is a common practice in climatology and is ecologically significant, for example, corals, chlorophyll, etc. are severely affected

Table 1a

Statistical indices for ROM, ESM and MME in reproducing the MHWs characteristics.

Statistical indices	ROM			ESM			MME		
	Event	Intensity	Duration	Event	Intensity	Duration	Event	Intensity	Duration
CC	0.85	0.86	0.89	0.81	0.83	0.86	0.83	0.77	0.87
RMSE	0.57	0.40	10.05	0.66	0.41	11.84	0.73	0.46	12.31
SS	0.56	0.69	0.98	0.65	0.71	1.25	0.71	0.80	1.20

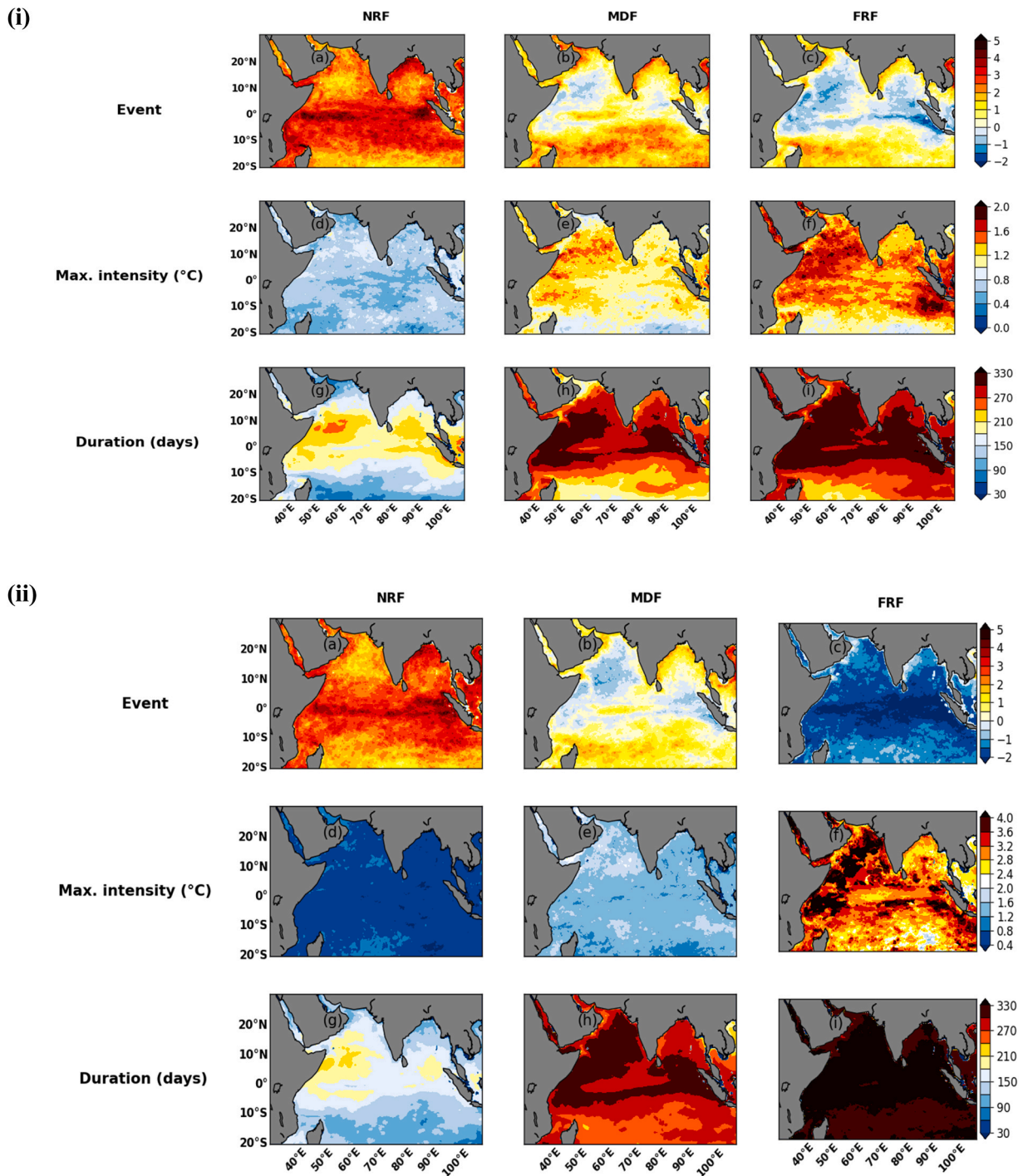


Fig. 4. Future changes in the MHWs metrics using (4(i)) RCP4.5 and (4(ii)) RCP8.5. For NRF (a, d, g), MDF (b, e, h), and FRF (c, f, i).

when SST reaches a specific threshold. Additionally, the capacity of the current ocean ecosystem to adjust to heat stress, computed with current threshold values, with acute and chronic impacts is largely known. That is why the future elevated temperatures can easily be translated into potential upcoming impacts on the ecosystem, whether steady and persistent or abrupt and temporary, with the use of the fixed baseline period. In the case of using varying baseline periods to define the MHWs, the threshold deleterious to the marine species remains unknown. Therefore, we stick to the utilization of a fixed threshold while highlighting the issue in the computation of future MHW events, which could be amended by the use of an updated standard definition in the computation of MHWs.

The MHWs intensity in both RCPs (Fig. 4(i)(d-f) and Fig. 4(ii)(d-f)) showed a continuous increase up to the end of the century, with an overall increase up to 2 °C (4 °C) in RCP4.5 (RCP8.5). In RCP4.5, the intensity in FRF (Fig. 4(i)(f)) is found to be more or less doubled of the NRF (Fig. 4(i)(d)), with some regional differences. However, in RCP8.5, a steep increase in the intensity with more than 8-fold from NRF to FRF period has been observed. In both scenarios, the maximum increase in intensity is evident over AS and Sumatra regions in all time slices.

In both RCPs, the MHWs duration is found to be increased during NRF (Fig. 4(i)(g) and Fig. 4(ii)(g)) showing a maximum increase over the western AS, GWP and Sumatra region (210 days). This enhancement in duration is further projected to accelerate in MDF following a similar spatial pattern of rising, having a maximum increase (>300days) around GWP and western AS. During FRF, in both RCPs, most regions of the TIO show an increase of 330 MHW days, indicating exposure of permanent MHW states by the 21st century (Fig. 4(i)(i) and Fig. 4(ii)(i)). Nevertheless, in the late future, the duration of MHW events is on the higher side in RCP8.5 than the RCP4.5.

It is imperative to note that the increase in the duration of events manifests the cause for the decrease in frequency during MDF and FRF in both RCP4.5 and RCP8.5 scenarios. Alternatively stated in MDF and FRF, there are no multiple short-duration events as in the historical period, instead a single big event that stands overlong and covers the everlasting duration of the year. Hence the number of MHW events per year is less, which on the further computation of change (MDF minus historical and FRF minus historical) shows a negative magnitude. The spatial patterns of the decrease (increase) in MHW events (intensity and duration) in all the time slices are analogous in RCP4.5 and RCP8.5, however, they differ in magnitude.

Additionally, the average proportion of TIO covered by different categories of MHWs, namely Moderate, Strong, Severe and Extreme, in the different time slices have been estimated, the results are summarized in Table 1b. Severe and Extreme MHWs were insignificant over the historical era, covering only 0.002 and 0.0001 proportion of the TIO respectively. In both RCPs, abrupt changes are noticed in the expansion of the MHW categories from NRF to late future, leading to de-escalation (escalation) of the Moderate and Strong MHWs (Severe and Extreme MHWs). Interestingly during FRF, explicitly, the Extreme category is dominant. Notably, nearly the entire TIO (~98%) will be covered with the Extreme category under RCP8.5 in FRF. On the other hand, in RCP 4.5, the Extreme category will constitute only ~49% of TIO.

This study investigated the spatial distribution of the appearance of the first permanent MHW states and absolute permanent MHW states (Fig. 5(a-d)). Strong spatial variability is noticed in the period of the first emergence of a permanent MHW state (Fig. 5(a-b)), ranging from 2010 to 2099 in both RCPs. For RCP8.5, the appearance of the first permanent MHW has been seen from 2010 over very few patches of AS, and by 2050 covering most of the central AS, GWP and southern BoB. The entrance of TIO into a permanent MHW state is in accordance with the latest Intergovernmental Panel on Climate Change (IPCC) report AR6 (Zhongming et al., 2021), which reported greater warming (1 °C) of the Indian Ocean than the global ocean (0.7 °C) during 1951–2015. Discernibly the appearance of the earliest first permanent MHW has been witnessed in RCP8.5 starting from 2015 and was over a few patches of AS. However, over a few regions of AS and BoB, the first permanent MHW has been observed earlier in RCP4.5 than in RCP8.5. A small region of Madagascar, north-west AS, and western BoB in the RCP4.5 does not exhibit the appearance of the first permanent MHW. However, these same areas have demonstrated a delayed appearance of the first permanent MHW under RCP8.5. Examining absolute permanent MHW under the RCP4.5 scenario (Fig. 5(c)) shows that only a few areas, mostly in the last decade of the century, will experience absolute permanent MHW conditions. These areas include Sumatra, southern BoB, GWP, and AS. While with the RCP8.5 scenario (Fig. 5(d)) AS, GWP and BoB will have absolute permanent MHW conditions starting from 2055 to 2070. Furthermore, Fig. 5(e-f) shows the proportion of TIO experiencing the first and absolute permanent MHW in both the RCPs. In RCP8.5, the first permanent MHW started in 2014 and subsequently increased over time to cover more than 98% of TIO before 2085. However, in RCP4.5, the first permanent started in 2015, covering a very small proportion (less than 5% of TIO), but a steady increase in proportion is evident from 2030, which covers 90% of TIO in the late century. In addition, the absolute permanent MHW in RCP4.5 was restricted to 10% of TIO only, which occurred from 2095 to 2100. While in RCP8.5, the absolute permanent MHW started in 2055 and augmented steadily, reaching more than 95% of TIO at the end of the century (Fig. 5(f)).

Substantial heterogeneity is found over TIO for frequency, intensity and the appearance of the first and absolute permanent MHW. Thus, we selected the regions of notable changes from TIO, which include AS, BoB and GWP. The annual mean MHWs intensity averaged over these regions is shown in Fig. 6(i), it can be noticed that their intensity shows a sharp continuous increase over time at each location with differences in magnitude in the RCP4.5 and RCP8.5 scenarios. It is also imperative to notice that the pattern of rising and falling in intensity with the advancing year is analogous at each location. To make results more discernible, the quantitative estimates of changes (explicitly manifesting the percentage change) in the intensity for the three time-slices relative to the historical

Table 1b
Average proportion of TIO experiencing different categories of MHWs in different time slices.

Time	The average proportion of TIO for MHWs categories in RCP4.5 (RCP8.5)			
	Moderate	Strong	Severe	Extreme
Historical	0.173	0.035	0.002	0.0001
NRF	0.305 (0.300)	0.309 (0.281)	0.160 (0.153)	0.070 (0.048)
MDF	0.147 (0.101)	0.234 (0.160)	0.319 (0.241)	0.306 (0.524)
FRF	0.089 (0.005)	0.158 (0.007)	0.281 (0.011)	0.492 (0.981)

Table 1: (a) Statistical indices of ROM, ESM and MME for MHWs and (b) mean proportion of TIO in different time slices with different categories of MHWs in ROM only within RCP4.5 (RCP8.5).

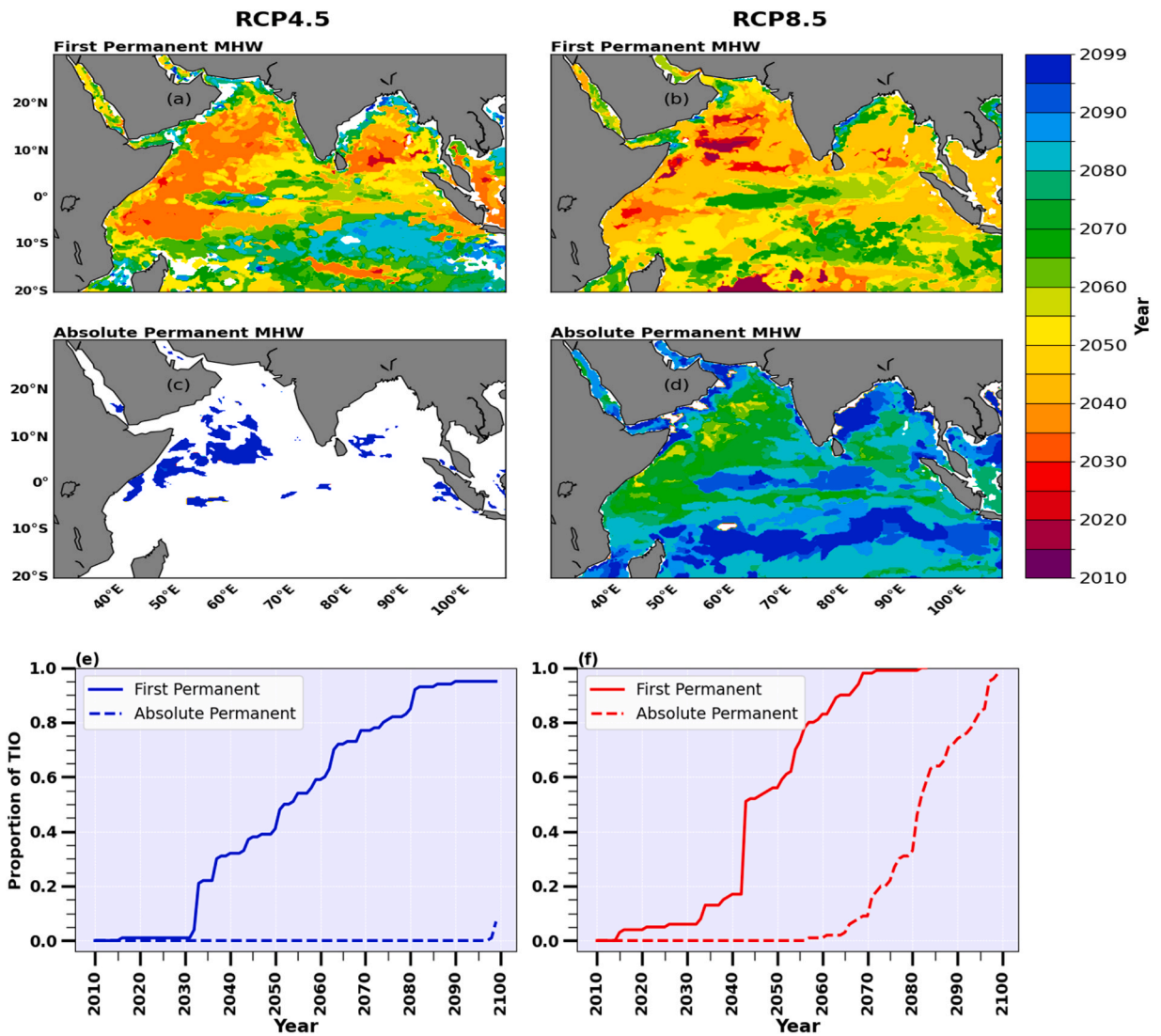
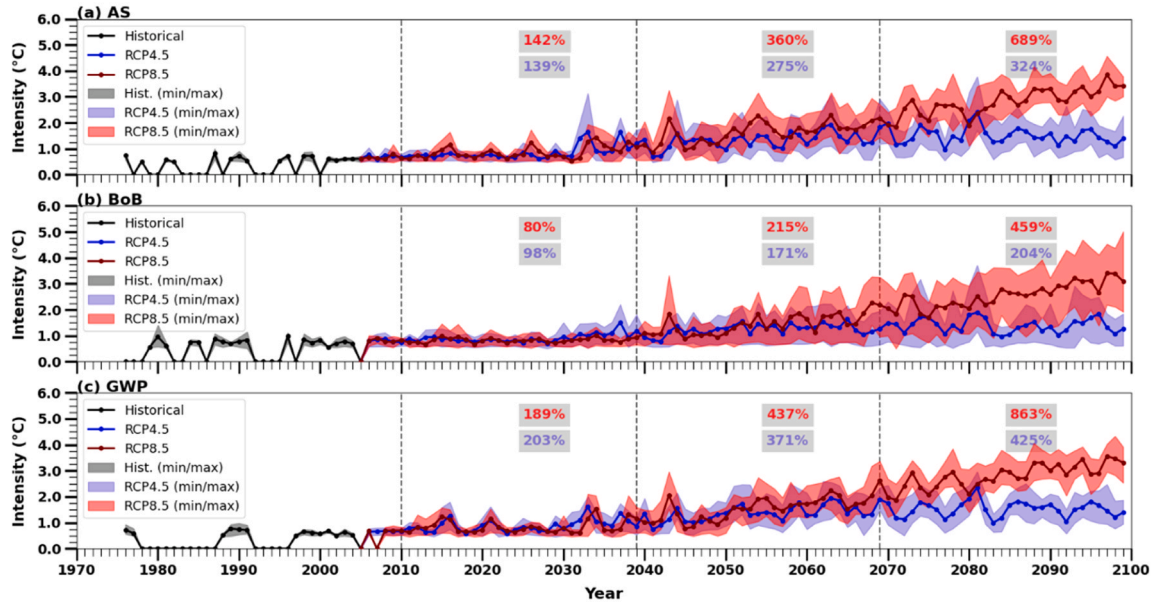


Fig. 5. Date of the first permanent MHW state (a-b), absolute permanent MHW state (c-d) and proportion of TIO under the first and the absolute permanent MHW state (e-f) in RCP4.5 and RCP8.5 scenarios.

(i)



(ii)

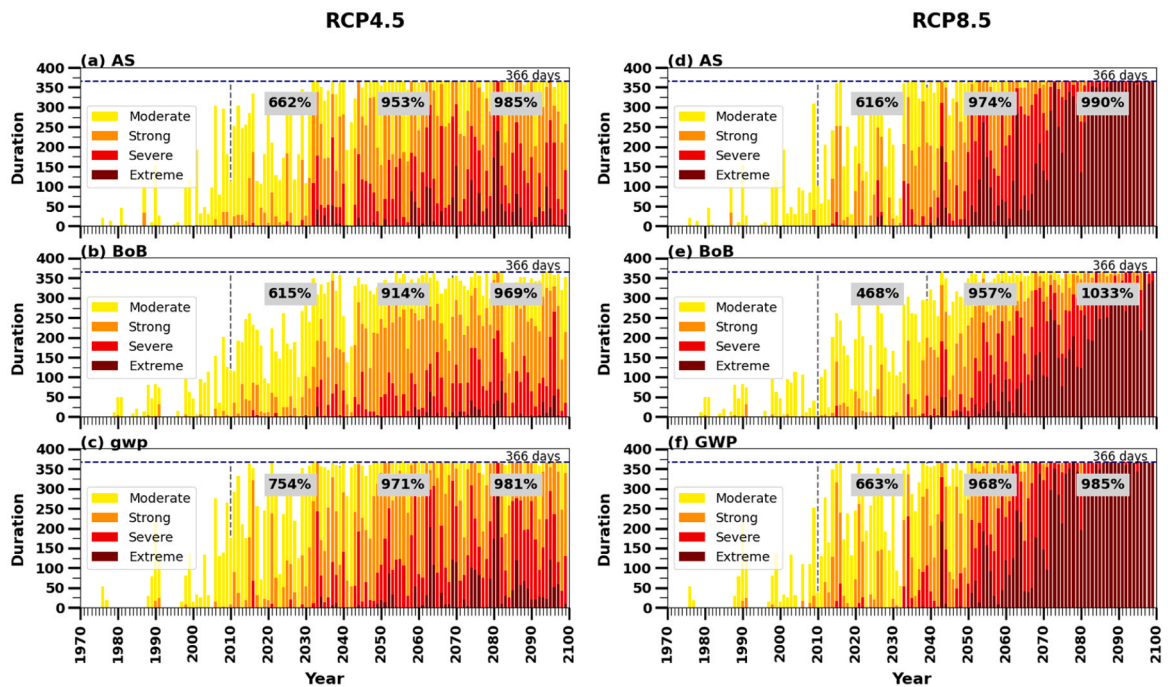


Fig. 6. The annual (6(i)) intensity and (6(ii)) duration of each MHWs category computed over AS, BoB and GWP using RCP4.5 and RCP8.5 scenarios.

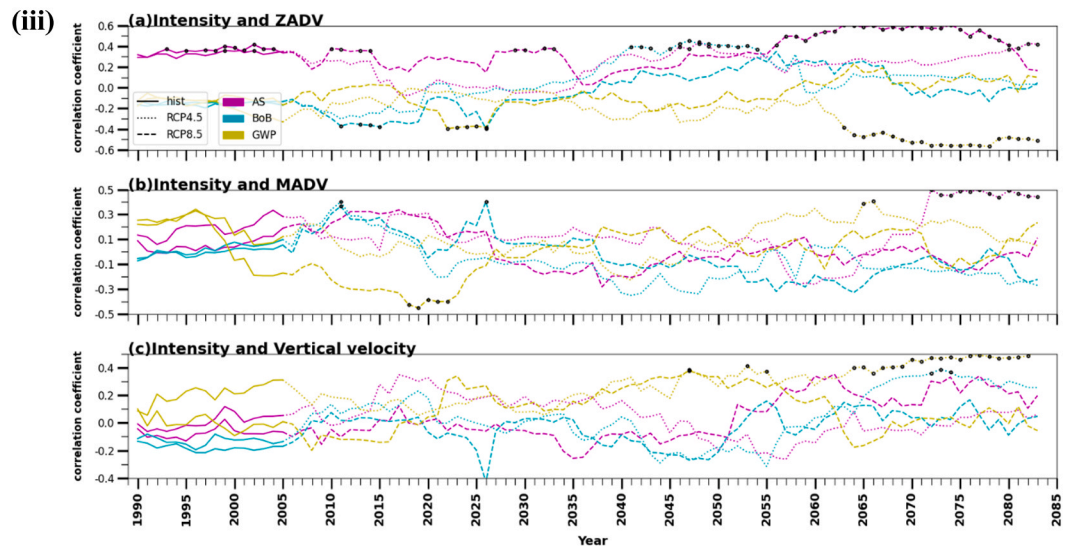
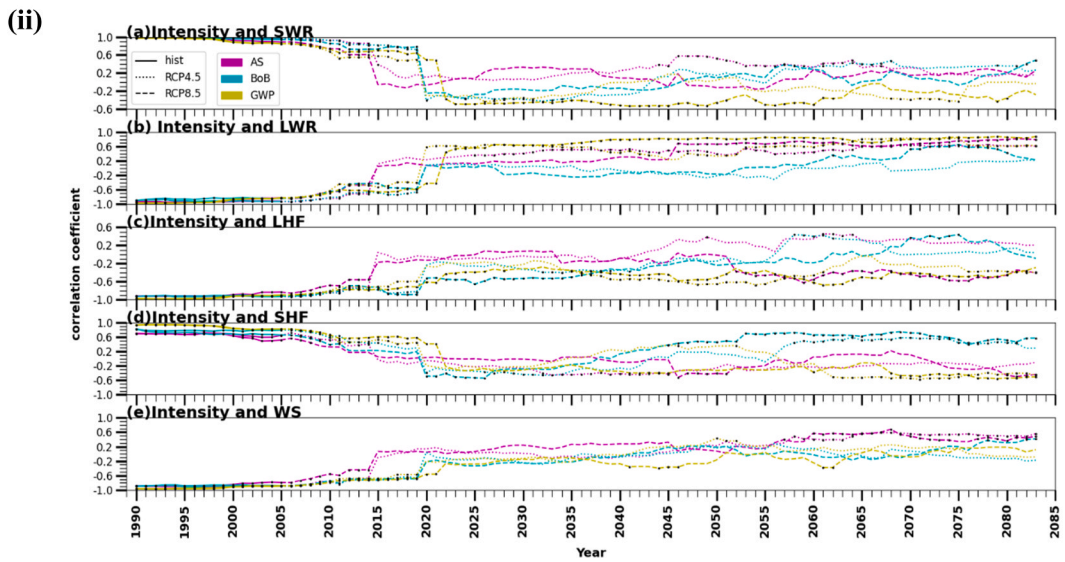
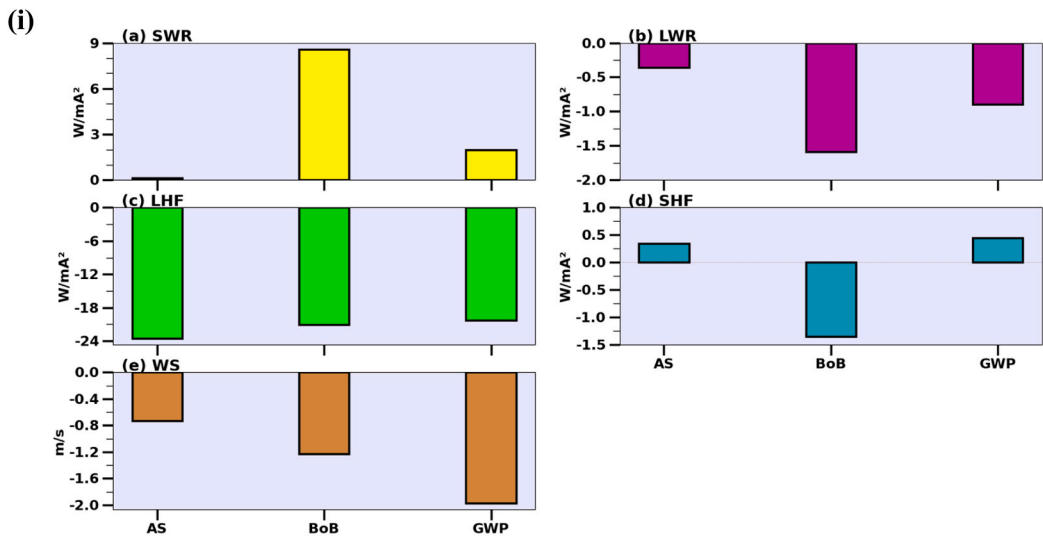


Fig. 7. (i) Changes in the Atmospheric parameters from their mean state 5 day before the genesis of MHWs. (ii) 31-year running correlation between atmospheric parameters and MHWs intensity. (iii) 31-year running correlation between heat budget terms and MHWs intensity. The black dots in the line represent where the running correlation value is at 95% significance level.

period have been made. Among the three locations, the rising rate in annual mean MHWs intensity at GWP is progressing much faster than in the other two locations. Roughly 4-fold (8-fold) multiplication in the intensity is evidenced over GWP during FRF with the RCP4.5 (RCP8.5) scenario.

Similarly, the annual duration of different categories of MHWs over AS, BoB and GWP has been shown as the stacked plots for RCP4.5 and RCP8.5 (Fig. 6(ii)). Over the years, the duration of events at each location is continually increasing, and in the long term, it ensures existence over the entire year. In RCP8.5, every location features a perpetual increase (decrease) in the duration of the Extreme (Moderate, Strong, Severe) category. In contrast, in RCP4.5 appearance of the Extreme category MHWs has been seen, which was nearly absent in the historical period. Notably, in RCP4.5, the strong and severe category MHWs covers the maximum days. The percentage change in the annual duration of MHWs in the three-time slices has been accounted for over all three locations in both the RCPs, which demonstrates a greater magnitude of increase in RCP8.5 than RCP4.5.

3.3. Causes for increased MHWs intensity

In Fig. 7(i) over AS, BoB and GWP the mean changes in atmospheric parameter 5-day before the genesis of all MHWs occurring during the historical period has been investigated. The MHW events start with an increase in the SWR and SHF, followed by a decrease in the LWR, LHF and WS, these all situations generate and maintain the MHWs situation, also reported in another study over TIO by

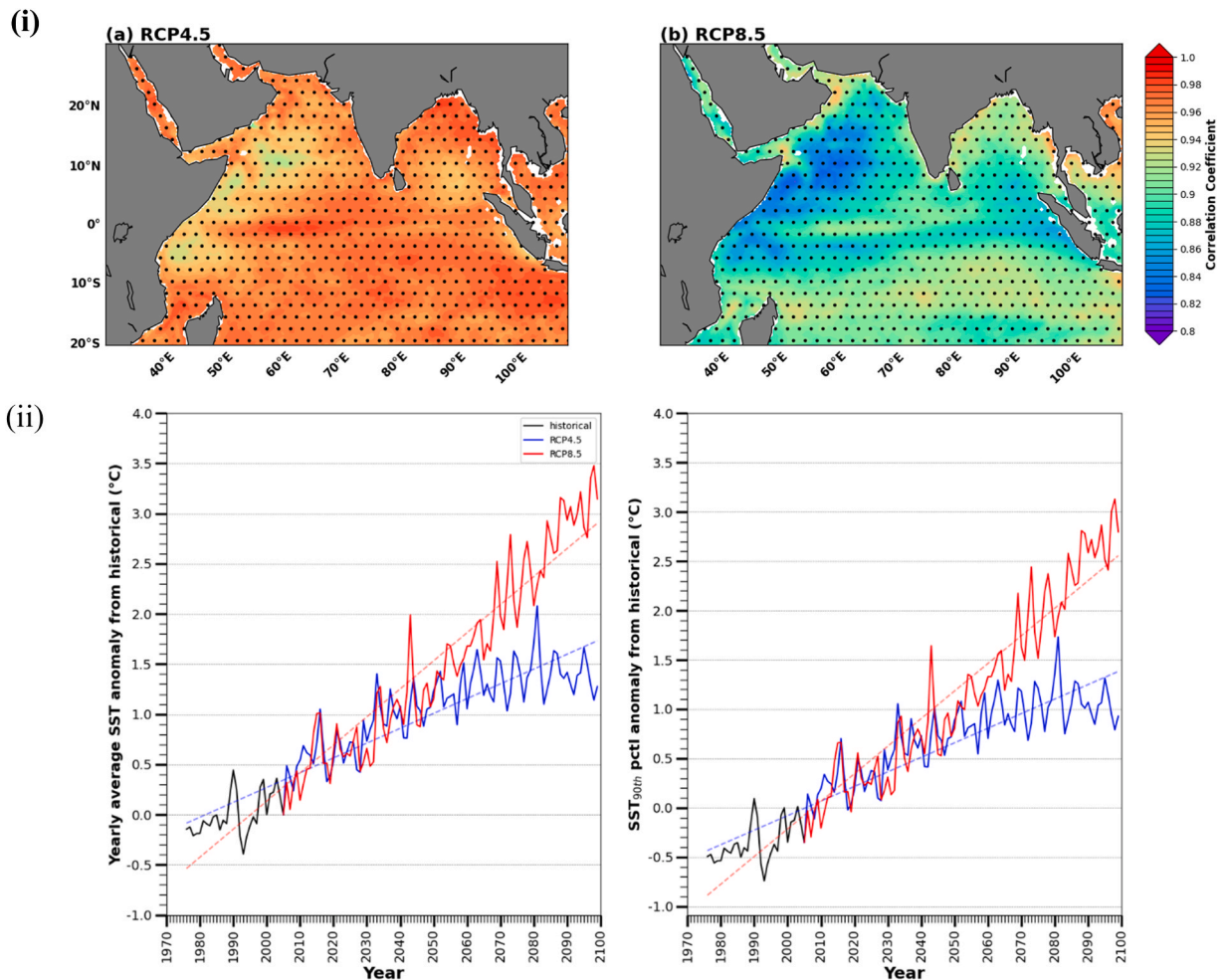


Fig. 8. (i) Correlation between mean SST anomaly and 90 percentile SST anomaly in both RCPs, anomaly computed with historical data (The regions with black dots represent significance level of more than 95%). (ii) Time series of area-averaged mean SST anomaly °C and 90 percentile SST anomaly °C anomaly computed with historical data.

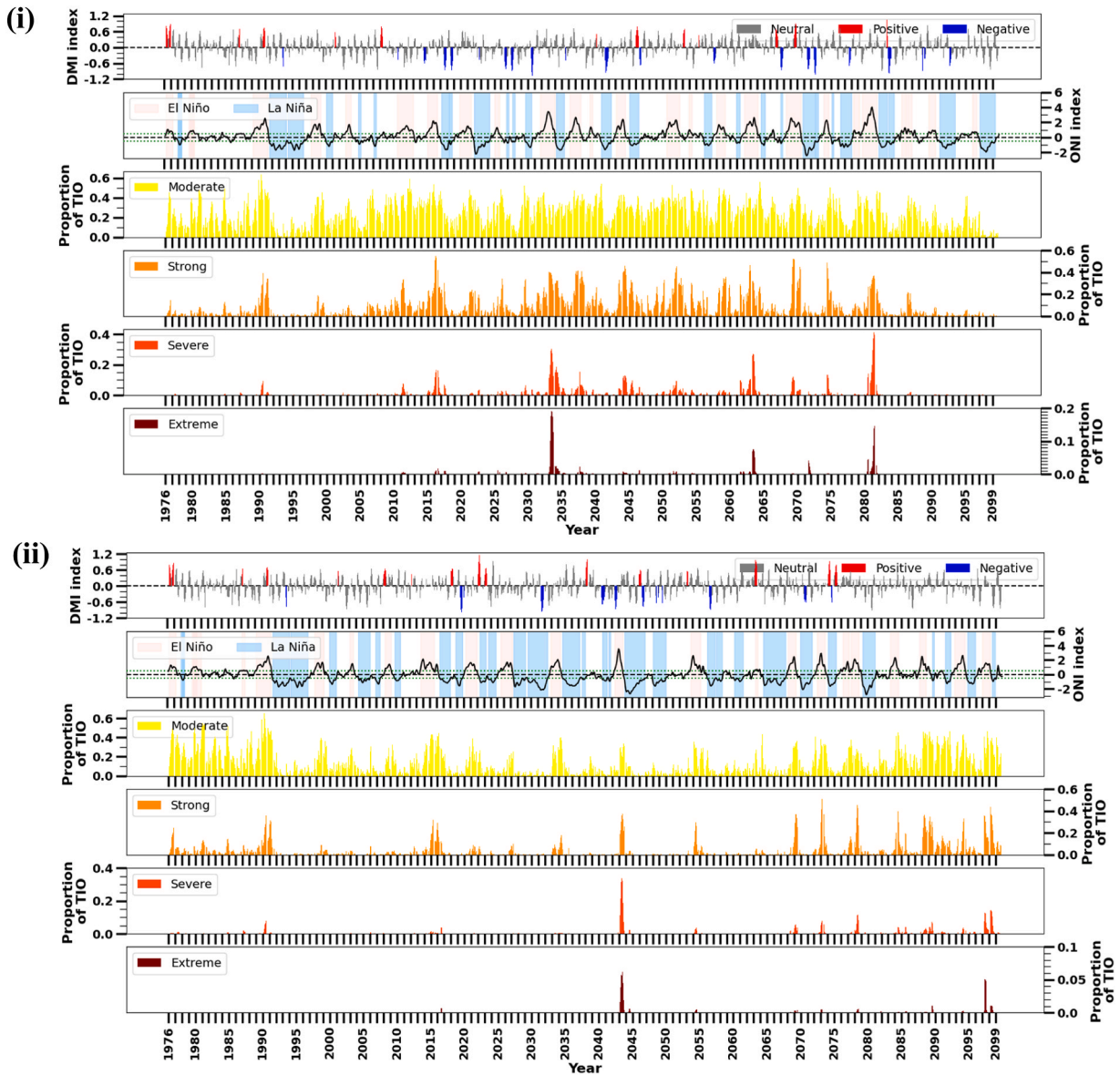


Fig. 9. ENSO and IOD modulation of MHWs severity. The proportion of the Moderate, Strong, Severe and Extreme category MHWs formed over TIO in (9(i)) RCP4.5 and (9(ii)) RCP8.5.

Saranya et al., 2022. The increased SWR accrues more heat to the surface, the decreased LWR prohibits the transfer of heat to the atmosphere, the decrease in WS results in the weakening of turbulence that inhibits mixing momentum transfer and restricts heat penetration into the deeper ocean. Further reduced evaporation (LHF) and increased SHF (except for the BoB; where the presence of both positive and negative anomalies in SHF during the MHW events, leading to a resultant negative anomaly might be because the model struggled to accurately capture the specific properties due to various complexities inherent in the region) restricts heat distribution. These all factors coherently lead to heat build-up in the upper ocean, contributing to the MHWs. A similar mechanism is also reported in the previous studies by Sen Gupta et al. (2020), Holbrook et al. (2019) and Saranya et al. (2022). It is imperative to note that, the magnitude of involved parameters for MHWs genesis varies with location. For example, the changes in SWR's for the genesis of MHWs are maximum over BoB similarly the drop in wind speed is maximum at GWP, Fig. 7(i).

Further, we calculated the running correlation of a 31-years moving window between the MHWs intensity and magnitude of these atmospheric parameters obtained during the MHW events, that is start date and end date of MHWs (Fig. 7 ii). Interestingly, the correlation (positive or negative) between the consistently increasing MHWs intensity and magnitude of atmospheric parameters remains on the higher side up to 2015, but after that, it started decreasing which might be due to the inclusion of warming in accordance with RCP4.5 and RCP8.5 scenarios. This decrease in correlation value indicates that the augmentation in the MHWs

intensity in the future is less dependent on the daily variation of these parameters. Moreover, the rolling correlation using a 31-years moving window has been computed between the annual intensity of MHWs and annual heat budget terms (Zonal advection (ZADV), Meridional advection (MADV) and vertical velocity). Notably, contrary to atmospheric parameters, the running correlation coefficient values are slightly lower with heat budget terms. This suggests that the future annual increase in MHWs intensity is less associated with these heat budget terms.

Darmaraki et al. (2019) demonstrated that the future increase in MHWs is largely attributed to the increased mean SST rather than day-to-day variability caused by the fluctuations in the parameters. Because the future's SST with the RCP scenarios in it will be higher than the historical SST threshold and hence there is a high tendency for future SST to easily cross the historical threshold defined for declaring the MHWs. The spatial plot in Fig. 8(i) demonstrates that there is a high correlation between the mean SST anomaly and 90th percentile anomaly from the historical for the entire study period (1976–2099) in the study domain. Further, the line plot of area-averaged TIO, Fig. 8(ii), shows that future 90th percentile SST are consistent with the rise in mean SST as the peaks and drops in mean SST anomaly and 90th percentile anomaly are highly analogous. It can further be observed that the value of the historical 90th percentile which constitutes MHWs in the historical period becomes a new normal in the future in response to increasing greenhouse gas forcing and therefore more intense MHWs in the future. This reconfirms the finding of Darmaraki et al. (2019).

3.4. IOD /ENSO

The TIO properties are strongly associated with various climatic modes, e.g. ENSO and IOD (Du et al., 2009; Saji et al., 1999; Sayantani and Gnanaseelan, 2015) and the warming of TIO following the El Niño years have been reported in the previous studies (Abish et al., 2018). This El Niño induced warming raises daily SST and might have implications on the MHW's characteristics. The additional warming introduced by El Niño will raise the daily SST above the threshold defined for declaring MHWs leading to prolonged and intense MHWs. Therefore, we use detrended SST data, to remove the long-term warming, for deriving ENSO and IOD index as well as the proportion of TIO experiencing different categories of MHWs.

Fig. 9(i) and (ii) show the proportion of the Moderate, Strong, Severe and Extreme category MHWs formed over TIO in RCP4.5 and RCP8.5 scenarios. Both the category and their proportion show a robust link with the El Niño events. During the El Niño years, the appearance of the Extreme category and an increase in the proportion of Moderate, Strong and Severe category MHWs is observed in both RCPs. In contrast in the La Niña years decrease in the proportion of MHWs category is evident. Moreover, such a strong inter-connection between the category of MHW events with DMI is not visible. Though, DMI eminently influences the MHWs in the proximity of the western box and eastern box during its positive and negative phases (Holbrook et al., 2019).

4. Conclusion

The anomalously warm conditions over the ocean known as marine heatwaves (MHWs) have deleterious impacts on regional ecosystems and have socioeconomic consequences. A new regional earth system model, ROM, driven by a global Earth System Model (MPI-ESM-LR) boundary conditions over CORDEX-South Asia, is employed to investigate the potential projected changes in the MHWs with respect to the historical period (1976–2005) as a baseline period for the near future (NRF; 2010–2039), middle future (MDF; 2040–2069), and far future (FRF; 2070–2099) under two emission scenarios (RCP4.5 and RCP8.5). The evaluation of the model's performance indicates a good resemblance between ROM and observation in reproducing the mean SST and MHWs during the historical period and outperforms the forcing model (MPI-ESM-LR) and Multi-Model Ensemble mean of CMIP5 models. After confirming the model's reliability for the historical climate, the projected change in the temperature extremes has been investigated. In the future, the duration and intensity of temperature extremes will escalate due to the continuous warming over most parts of TIO, with the highest warming over AS followed by GWP and BoB. Notably, the magnitude of MHWs intensity and duration is significantly higher in RCP8.5 than in RCP4.5, primarily due to a higher degree of warming. A considerable departure from the historical conditions leads to the development of permanent MHW states in the future that might impose abrupt ecological changes impacting marine species. The AS and GWP regions will experience the first permanent MHW and absolute permanent MHW events at the earliest period. The absolute permanent MHW state is largely visible in RCP8.5, while in RCP4.5, it is restricted to some regions of AS and GWP only, particularly in the late century. The decline in WS, LHF, and increase in SWR primarily manifest the establishment of MHW conditions. Running correlation reveals that the atmospheric parameters, vertical velocity, and zonal and meridional advection have a good correlation with intensity but in the long future term rise in mean SST plays a major role than the variability in these parameters for rising MHW intensity. During the El Niño regime, not only the proportion of TIO experiencing MHWs increase, but also the appearance of higher category MHWs is evident. IOD controls the MHWs metrics in the proximity of the western box and eastern box during positive and negative phases. In summary, this study discovered that in both RCPs, MHW is projected to be more prolonged and intense, covering a wider spatial area, along with exposure of TIO to the permanent MHW.

Data Availability Statement

The authors are thankful to the National Oceanic and Atmospheric Administration (NOAA) for freely available daily Sea Surface Temperature data, which can be derived using this link <https://psl.noaa.gov/data/gridded/data.noaa.oisst.v2.highres.html> and model data would be made available upon request to the corresponding author.

Funding

This work is supported by the Department of Science and Technology (DST), Govt. of India, grant number DST/INT/RUS/RSF/P-33/G. AKM, LKP and ASD acknowledge the DST for funding the fellowship. DVS and VAR were supported in the framework of SIO RAS state assignment (theme No. FMWE-2021-0014). DVS also acknowledges the funding by the Federal Ministry of Education and Research of Germany (BMBF) in the framework of ACE (grant 01LP2004A). Simulations were performed on the German Climate Computing Center (DKRZ) under grant number ba1144.

CRedit authorship contribution statement

PK and ASD designed the study and wrote the first draft of the manuscript. ASD did all the analysis under the guidance of PK and in consultation with AKM. All the authors discussed the results and jointly contributed to the editing and formulation of the final manuscript.

Declaration of Competing Interest

The authors declare that they have no known competing financial interests or personal relationships that could have appeared to influence the work reported in this paper.

Data Availability

Data will be made available on request.

References

- Abish, B., Cherchi, A., Ratna, S.B., 2018. ENSO and the recent warming of the Indian Ocean. *Int. J. Climatol.* 38 (1), 203–214.
- Alexander, M.A., Scott, J.D., Friedland, K.D., Mills, K.E., Nye, J.A., Pershing, A.J., Thomas, A.C., 2018. Projected sea surface temperatures over the 21st century: Changes in the mean, variability and extremes for large marine ecosystem regions of Northern Oceans. *Elementa* 6. <https://doi.org/10.1525/ELEMENTA.191/471549/191-4558-1-PB.PDF>.
- Amaya, D., Jacox, M.G., Fewings, M.R., Saba, V.S., Stuecker, M.F., Rykaczewski, R.R., Powell, B.S., 2023. Marine heatwaves need clear definitions so coastal communities can adapt. *Nature* 616 (7955), 29–32.
- Bates, A., Hilton, B., Harley, C., 2009. Effects of temperature, season and locality on wasting disease in the keystone predatory sea star *Pisaster ochraceus*. *Dis. Aquat. Org.* 86 (3), 245–251. <https://doi.org/10.3354/DAO02125>.
- Benthuyesen, J.A., Oliver, E.C.J., Chen, K., Wernberg, T., 2020. Editorial: advances in understanding marine heatwaves and their impacts. *Front. Mar. Sci.* 0, 147. <https://doi.org/10.3389/FMARS.2020.00147>.
- Bond, N.A., Cronin, M.F., Freeland, H., Mantua, N., 2015. Causes and impacts of the 2014 warm anomaly in the NE Pacific. *Geophys. Res. Lett.* 42 (9), 3414–3420. <https://doi.org/10.1002/2015GL063306>.
- Chakraborty, A., Chandrakar, R., Kumar, S., Sadhukhan, B., Kumar, A., 2023. Analysis of marine heatwaves and biogeochemistry in the Northern Arabian Sea. *Reg. Stud. Mar. Sci.*, 103019.
- Chatterjee, A., Anil, G., Shenoy, L.R., 2022. Marine heatwaves in the Arabian Sea. *Ocean Sci.* 18 (3), 639–657.
- Chen, K., Gawarkiewicz, G.G., Lentz, S.J., Bane, J.M., 2014. Diagnosing the warming of the Northeastern U.S. Coastal Ocean in 2012: A linkage between the atmospheric jet stream variability and ocean response. *J. Geophys. Res.: Oceans* 119 (1), 218–227. <https://doi.org/10.1002/2013JC009393>.
- Darmaraki, S., Somot, S., Sevault, F., Nabat, P., Cabos Narvaez, W.D., Cavicchia, L., et al., 2019. Future evolution of Marine Heatwaves in the Mediterranean Sea. *Clim. Dyn.* 53 (3–4), 1371–1392. <https://doi.org/10.1007/S00382-019-04661-Z/FIGURES/13>.
- Darmaraki, S., Somot, S., Sevault, F., Nabat, P., 2019. Past variability of mediterranean sea marine heatwaves. *Geophys. Res. Lett.* 46 (16), 9813–9823. <https://doi.org/10.1029/2019GL082933>.
- Dubey, A.K., Lal, P., Kumar, P., Kumar, A., Dvornikov, A.Y., 2021. Present and future projections of heatwave hazard-risk over India: a regional earth system model assessment. *Environ. Res.* 201, 111573.
- Du, Y., Xie, S.-P., Huang, G., Hu, K., 2009. Role of Air–Sea Interaction in the Long Persistence of El Niño–Induced North Indian Ocean Warming. *J. Clim.* 22 (8), 2023–2038. <https://doi.org/10.1175/2008JCLI2590.1>.
- Dwivedi, S., Srivastava, A., & Mishra, A.K. (2017). Upper Ocean Four-Dimensional Variational Data Assimilation in the Arabian Sea and Bay of Bengal. *https://doi.org/10.1080/01490419.2017.1405128*, 41(3), 230–257 <https://doi.org/10.1080/01490419.2017.1405128>.
- Feng, M., McPhaden, M.J., Xie, S.-P., Hafner, J., 2013. La Niña forces unprecedented Leeuwin Current warming in 2011. *2013 3:1 Sci. Rep.* 3 (1), 1–9. <https://doi.org/10.1038/srep01277>.
- Feng, M., Hendon, H.H., Xie, S.P., Marshall, A.G., Schiller, A., Kosaka, Y., Pearce, A., 2015. Decadal increase in Ningaloo Niño since the late 1990s. *Geophysical Research Letters*, 42(1), 104–112.
- Frölicher, T.L., Fischer, E.M., Gruber, N., 2018. Marine heatwaves under global warming. *2018 560:7718 Nature* 560 (7718), 360–364. <https://doi.org/10.1038/s41586-018-0383-9>.
- Garrabou, J., Coma, R., Bensoussan, N., Bally, M., Chevaldonné, P., Cigliano, M., et al., 2009. Mass mortality in Northwestern Mediterranean rocky benthic communities: effects of the 2003 heat wave. *Glob. Change Biol.* 15 (5), 1090–1103. <https://doi.org/10.1111/J.1365-2486.2008.01823.X>.
- Giorgi, F., GAO, X.J., 2018. Regional earth system modeling: review and future directions. *Atmos. Ocean. Sci. Lett.* 11 (2), 189–197.
- Glantz, M.H., Ramirez, L.J., 2020. Reviewing the Oceanic Niño Index (ONI) to enhance societal readiness for El Niño's Impacts. *Int. J. Disaster Risk Sci.* Vol. <https://doi.org/10.1007/s13753-020-00275-w>.
- Gnanaseelan, C., Roxy, M.K., Deshpande, A., 2017. Variability and trends of sea surface temperature and circulation in the Indian Ocean. *Springer Geol.* 165–179. https://doi.org/10.1007/978-981-10-2531-0_10.
- Sen Gupta, A., Thomsen, M., Benthuyesen, J.A., Hobday, A.J., Oliver, E., Alexander, L.V., et al., 2020. Drivers and impacts of the most extreme marine heatwaves events. *Sci. Rep.* 10 (1) <https://doi.org/10.1038/s41598-020-75445-3>.
- Hagemann, S., Dümenil, L., 1998. A parameterization of the lateral waterflow for the global scale. *Clim. Dyn.* 14, 17–31.
- Hayashida, H., Matear, R.J., Strutton, P.G., 2020. Background nutrient concentration determines phytoplankton bloom response to marine heatwaves. *Glob. Change Biol.* 26 (9), 4800–4811. <https://doi.org/10.1111/GCB.15255>.
- Hobday, A.J., Alexander, L.V., Perkins, S.E., Smale, D.A., Straub, S.C., Oliver, E.C.J., et al., 2016. A hierarchical approach to defining marine heatwaves. *Prog. Oceanogr.* 141, 227–238. <https://doi.org/10.1016/J.POCEAN.2015.12.014>.

- Hobday, A.J., Oliver, E.C.J., Gupta, A., Sen, Benthuyens, J.A., Burrows, M.T., Donat, M.G., et al., 2018. Categorizing and naming marine heatwaves. *Oceanography* 31 (2 Special Issue), 162–173. <https://doi.org/10.5670/oceanog.2018.205>.
- Holbrook, N.J., Scannell, H.A., Sen Gupta, A., Benthuyens, J.A., Feng, M., Oliver, E.C.J., et al., 2019. A global assessment of marine heatwaves and their drivers. *2019 10:1 Nat. Commun.* 10 (1), 1–13. <https://doi.org/10.1038/s41467-019-10206-z>.
- Holbrook, N.J., Hernaman, V., Koshiba, S., Lako, J., Kajtar, J.B., Amosa, P., Singh, A., 2022. Impacts of marine heatwaves on tropical western and central Pacific Island nations and their communities. *Glob. Planet. Change* 208, 103680. <https://doi.org/10.1016/j.gloplacha.2021.103680>.
- Hu, S., Li, S., Zhang, Y., Guan, C., Du, Y., Feng, M., et al., 2021. Observed strong subsurface marine heatwaves in the tropical western Pacific Ocean. *Environ. Res. Lett.* 16 (10), 104024 <https://doi.org/10.1088/1748-9326/AC26F2>.
- Jacob, D., 2001. A note to the simulation of the annual and inter-annual variability of the water budget over the Baltic Sea drainage basin. *Meteorol. Atmos. Phys.* 77 (1–4), 61–73. <https://doi.org/10.1007/S007030170017>.
- Jacob, D., Podzun, R., 1997. Sensitivity studies with the regional climate model REMO, 1997 63:1 *Meteorol. Atmos. Phys.* 63 (1), 119–129. <https://doi.org/10.1007/BF01025368>.
- Jungclaus, J.H., Fischer, N., Haak, H., Lohmann, K., Marotzke, J., Matei, D., et al., 2013. Characteristics of the ocean simulations in the Max Planck Institute Ocean Model (MPIOM) the ocean component of the MPI-Earth system model. *J. Adv. Model. Earth Syst.* 5 (2), 422–446. <https://doi.org/10.1002/JAME.20023>.
- Kataoka, T., Tozuka, T., Behera, S., Yamagata, T., 2014. On the ningaloo niño/niña. *Clim. Dyn.* 43, 1463–1482.
- Kumar, P., Sein, D., Cabos, W., Jacob, D., 2014a. Improved precipitation extremes and climatology in a regional coupled model simulation over CORDEX South Asia domain. AGU Fall Meeting. (<https://agu.confex.com/agu/fm14/meetinga>) pp.cgi/Paper/16921.
- Kumar, P., Sein, D., Cabos, W., Jacob, D., 2014b. Improvement of simulated monsoon precipitation over South Asia with a regionally coupled model ROM. In: Barring, L., Reckermann, M., Rockel, B., Rummukainen, M. (Eds.), 3rd International Lund Regional-Scale Climate Modelling Workshop 21st Century Challenges in Regional Climate Modelling: Workshop proceedings, Lund, Sweden.
- Kumar, P., Mishra, A.K., Dubey, A.K., Javed, A., Saharwardi, M.S., Kumari, A., et al., 2022. Regional earth system modelling framework for CORDEX-SA: an integrated model assessment for Indian summer monsoon rainfall. *Clim. Dyn.* 1, 1–20. <https://doi.org/10.1007/S00382-022-06217-0/FIGURES/2>.
- Kumar, P., Javed, A., Kolli, R.K., Sachan, D., Dinesh, A.S., Murukesh, M., Mishra, G., 2023. National colloquium for advances in weather and climate prediction and climate change projection over south asia: applications in water and agriculture sectors. *Bull. Am. Meteorol. Soc.* 104 (9), E1564-E1569.
- Kumari, A., Kumar, P., 2023. Evaluation and future projection of the extreme precipitation over India and its homogeneous regions: a regional earth system model perspective. *Int. J. Climatol.* 43 (8), 3679–3697.
- Di Lorenzo, E., Mantua, N., 2016. Multi-year persistence of the 2014/15 North Pacific marine heatwave. *Nat. Clim. Change* 6 (11), 1042–1047. <https://doi.org/10.1038/nclimate3082>.
- Maier-Reimer, E., I. Kriest, J. Segsneider, P. Wetzel, 2005. Technical description of the Hamburg Ocean Carbon Cycle model, version 5.1 (HAMOCC5.1), and of its interface to MPIOM. Reports on Earth System Science, Max Planck Institute for Meteorol., Hamburg. [Available at <http://edoc.mpg.de/get.php?fid517575&did5249293&ver50>].
- Manta, G., Mello, S., de, Trinchini, R., Badagian, J., Barreiro, M., 2018. The 2017 record marine heatwave in the southwestern atlantic shelf, 12,449–12,456 *Geophys. Res. Lett.* 45 (22). <https://doi.org/10.1029/2018GL081070>.
- Marshall, A.G., Hendon, H.H., Feng, M., Schiller, A., 2015. Initiation and amplification of the Ningaloo Niño. *Clim. Dyn.* 45, 2367–2385.
- McCabe, R.M., Hickey, B.M., Kudela, R.M., Lefebvre, K.A., Adams, N.G., Bill, B.D., et al., 2016. An unprecedented coastwide toxic algal bloom linked to anomalous ocean conditions, 10,366–10,376 *Geophys. Res. Lett.* 43 (19). <https://doi.org/10.1002/2016GL070023>.
- Mishra, A.K., Kumar, P., Dubey, A.K., Javed, A., Saharwardi, M.S., Sein, D.V., et al., 2021. Impact of horizontal resolution on monsoon precipitation for CORDEX-South Asia: A regional earth system model assessment. *Atmos. Res.* 259, 105681 <https://doi.org/10.1016/j.atmosres.2021.105681>.
- Mishra, A.K., Dwivedi, S., Di Sante, F., 2021. Performance of the RegCM-MITgcm coupled regional model in simulating the indian summer monsoon rainfall, 2021 178:2 *Pure Appl. Geophys.* 178 (2), 603–617. <https://doi.org/10.1007/S00024-020-02648-0>.
- Mishra, A.K., Dubey, A.K., Dinesh, A.S., 2023. Diagnosing whether the increasing horizontal resolution of regional climate model inevitably capable of adding value: investigation for Indian summer monsoon. *Clim. Dyn.* 60 (7–8), 1925–1945.
- NOAA. (2022). Climate Prediction Center - ONI. Retrieved February 1, 2022, from (https://origin.cpc.ncep.noaa.gov/products/analysis_monitoring/ensostuff/ONI_v5.php).
- Le Nohaïc, M., Ross, C.L., Cornwall, C.E., Comeau, S., Lowe, R., McCulloch, M.T., Schoepf, V., 2017. Marine heatwave causes unprecedented regional mass bleaching of thermally resistant corals in northwestern Australia. *2017 7:1, Sci. Rep.* 7 (1), 1–11. <https://doi.org/10.1038/s41598-017-14794-y>.
- Oliver, E.C.J., Burrows, M.T., Donat, M.G., Sen Gupta, A., Alexander, L.V., Perkins-Kirkpatrick, S.E., et al., 2019. Projected marine heatwaves in the 21st century and the potential for ecological impact. *Front. Mar. Sci.* 6 (December), 1–12. <https://doi.org/10.3389/fmars.2019.00734>.
- Oliver, E.C., Benthuyens, J.A., Darmaraki, S., Donat, M.G., Hobday, A.J., Holbrook, N.J., ... & Sen Gupta, A. (2021). Marine heatwaves. *Annual Review of Marine Science*, 13, 313–342.
- Pandey, L.K., Dwivedi, S., 2021. Comparing the performance of turbulent kinetic energy and K-profile parameterization vertical parameterization schemes over the Tropical Indian Ocean. *Mar. Geod.* 44 (1), 42–69. <https://doi.org/10.1080/01490419.2020.1835758>.
- Pandey, L.K., Dwivedi, S., Martin, M., 2021. Short-term predictability of the bay of Bengal region using a high-resolution Indian Ocean Model. *Mar. Geod.* 44 (3), 215–237. <https://doi.org/10.1080/01490419.2021.1894273>.
- Pearce, A.F., Feng, M., 2013. The rise and fall of the “marine heat wave” off Western Australia during the summer of 2010/2011. *J. Mar. Syst.* 111–112, 139–156. <https://doi.org/10.1016/j.jmarsys.2012.10.009>.
- Plecha, S.M., Soares, P.M.M., 2020. Global marine heatwave events using the new CMIP6 multi-model ensemble: from shortcomings in present climate to future projections. *Environ. Res. Lett.* 15 (12), 124058 <https://doi.org/10.1088/1748-9326/ABC847>.
- Rathore, S., Goyal, R., Jangir, B., Ummeenhofer, C.C., Feng, M., Mishra, M., 2022. Interactions between a marine heatwave and Tropical Cyclone Amphan in the Bay of Bengal in 2020. *Front. Clim.* 4, 861477.
- Reynolds, R.W., Smith, T.M., Liu, C., Chelton, D.B., Casey, K.S., Schlax, M.G., 2007. Daily high-resolution-blended analyses for sea surface temperature. *J. Clim.* 20 (22), 5473–5496. <https://doi.org/10.1175/2007JCLI1824.1>.
- Rodrigues, R.R., Taschetto, A.S., Sen Gupta, A., Foltz, G.R., 2019. Common cause for severe droughts in South America and marine heatwaves in the South Atlantic. *2019 12:8 Nat. Geosci.* 12 (8), 620–626. <https://doi.org/10.1038/s41561-019-0393-8>.
- Roxy, M., Tanimoto, Y., 2007. Role of SST over the Indian Ocean in influencing the intraseasonal variability of the Indian summer monsoon. *J. Meteorol. Soc. Jpn.* 85 (3), 349–358. <https://doi.org/10.2151/JMSJ.85.349>.
- Roxy, M., Tanimoto, Y., Preethi, B., Terray, P., Krishnan, R., 2012. Intraseasonal SST-precipitation relationship and its spatial variability over the tropical summer monsoon region. *2012 41:1 Clim. Dyn.* 41 (1), 45–61. <https://doi.org/10.1007/S00382-012-1547-1>.
- Roxy, M.K., Modi, A., Murtugudde, R., Valsala, V., Panickal, S., Kumar, S.P., et al., 2016. A reduction in marine primary productivity driven by rapid warming over the tropical Indian Ocean. *Geophys. Res. Lett.* 43 (2), 826–833. <https://doi.org/10.1002/2015GL066979>.
- Saji, N.H., Goswami, B.N., Vinayachandran, P.N., Yamagata, T., 1999. A dipole mode in the tropical Indian Ocean. *1999 401:6751 Nature* 401 (6751), 360–363. <https://doi.org/10.1038/43854>.
- Di Sante, F., Coppola, E., Farneti, R., Giorgi, F., 2019. Indian Summer Monsoon as simulated by the regional earth system model RegCM-ES: the role of local air–sea interaction. *2019 53:1 Clim. Dyn.* 53 (1), 759–778. <https://doi.org/10.1007/S00382-019-04612-8>.
- Saharwardi, M.S., Kumar, P., Sachan, D., 2021. Evaluation and projection of drought over India using high-resolution regional coupled model ROM. *Clim. Dyn.* 1–19.
- Saranya, J.S., Roxy, M.K., Dasgupta, P., Anand, A., 2022. Genesis and Trends in Marine Heatwaves Over the Tropical Indian Ocean and Their Interaction With the Indian Summer Monsoon. *e2021JC017427 J. Geophys. Res.: Oceans* 127 (2). <https://doi.org/10.1029/2021JC017427>.
- Sayantani, O., Gnanaseelan, C., 2015. Tropical Indian Ocean subsurface temperature variability and the forcing mechanisms. *Clim. Dyn.* 44 (9–10), 2447–2462. <https://doi.org/10.1007/S00382-014-2379-Y/FIGURES/12>.

- Schaeffer, A., Roughan, M., 2017. Subsurface intensification of marine heatwaves off southeastern Australia: the role of stratification and local winds. *Geophys. Res. Lett.* 44 (10), 5025–5033. <https://doi.org/10.1002/2017GL073714>.
- Sein, D.V., Mikolajewicz, U., Gröger, M., Fast, I., Cabos, W., Pinto, J.G., et al., 2015. Regionally coupled atmosphere-ocean-sea ice-marine biogeochemistry model ROM: 1. Description and validation. *J. Adv. Model. Earth Syst.* 7 (1), 268–304. <https://doi.org/10.1002/2014MS000357>.
- Sein, D.V., Gröger, M., Cabos, W., Alvarez-García, F.J., Hagemann, S., Pinto, J.G., et al., 2020. Regionally coupled atmosphere-ocean-marine biogeochemistry model rom: 2. studying the climate change signal in the north Atlantic and Europe. e2019MS001646 *J. Adv. Model. Earth Syst.* 12 (8). <https://doi.org/10.1029/2019MS001646>.
- Sein, D.V., Dvornikov, A.Y., Martyanov, S.D., Cabos, W., Ryabchenko, V.A., Gröger, M., Jacob, D., Kumar Mishra, A., Kumar, P., 2022. Indian Ocean marine biogeochemical variability and its feedback on simulated South Asia climate. *Earth Syst. Dynam.* 13, 809–831. <https://doi.org/10.5194/esd-13-809-2022>.
- Singh, C., Dasgupta, P., 2017. Unraveling the spatio-temporal structure of the atmospheric and oceanic intra-seasonal oscillations during the contrasting monsoon seasons. *Atmos. Res.* 192, 48–57. <https://doi.org/10.1016/J.ATMOSRES.2017.03.020>.
- Smale, D.A., Wernberg, T., Oliver, E.C.J., Thomsen, M., Harvey, B.P., Straub, S.C., et al., 2019. Marine heatwaves threaten global biodiversity and the provision of ecosystem services. *Nat. Clim. Change* 9 (4), 306–312. <https://doi.org/10.1038/s41558-019-0412-1>.
- Srivastava, A., Dwivedi, S., Mishra, A.K. 2016. Intercomparison of High-Resolution Bay of Bengal Circulation Models Forced with Different Winds. <http://Dx.Doi.Org/10.1080/01490419.2016.1173606>, 39(3–4), 271–289. (<https://doi.org/10.1080/01490419.2016.1173606>).
- Srivastava, A., Dwivedi, S., Mishra, A.K., 2018. Investigating the role of air-sea forcing on the variability of hydrography, circulation, and mixed layer depth in the Arabian Sea and Bay of Bengal. *Oceanologia* 60 (2), 169–186. <https://doi.org/10.1016/J.OCEANO.2017.10.001>.
- Suneet, D., Kumar, M.A., Atul, S., 2019. Upper ocean high resolution regional modeling of the Arabian Sea and Bay of Bengal. 2019 38:5 *Acta Oceanol. Sin.* 38 (5), 32–50. <https://doi.org/10.1007/S13131-019-1439-X>.
- Vialard, J., Delecluse, P., 1998. An OGCM study for the TOGA decade. part ii: barrier-layer formation and variability | semantic scholar. *J. Phys. Oceanogr.* 28 (6), 1071–1088. <https://www.semanticscholar.org/paper/An-OGCM-Study-for-the-TOGA-Decade-Part-II%3A-and-Vialard-Delecluse/06bd29d265734e1764332c1859a4019cb3531b7b>.
- Vialard, J., Menkes, C., Boulanger, J.-P., Delecluse, P., Guilyardi, E., McPhaden, M.J., Madec, G., 2001. A model study of oceanic mechanisms affecting Equatorial Pacific sea surface temperature during the 1997-98 El Niño. *El Niño. J. Phys. Oceanogr.* 7, 1649–1675. <https://doi.org/10.1175/1520.1119-1129>. <https://doi.org/10.1007/S00704-021-03591-3/FIGURES/8>.
- Van Viet, L., 2021. Development of a new ENSO index to assess the effects of ENSO on temperature over southern Vietnam. *Theor. Appl. Climatol.* 144 (3–4), 1119–1129. <https://doi.org/10.1007/S00704-021-03591-3/FIGURES/8>.
- Zhongming, Z., Linong, L., Wangqiang, Z., Wei, L., 2021. AR6 Climate Change 2021: The Physical Science Basis. Retrieved from (<http://119.78.100.173/C666/handle/2XK7JSWQ/270167>).
- Zhu, S., Remedio, A.R.C., Sein, D.V., Sielmann, F., Ge, F., Xu, J., et al., 2020. Added value of the regionally coupled model ROM in the East Asian summer monsoon modeling. *Theor. Appl. Climatol.* 140 (1–2), 375–387. <https://doi.org/10.1007/S00704-020-03093-8>.
- Zhu, X., Wei, Z., Dong, W., Ji, Z., Wen, X., Zheng, Z., et al., 2020. Dynamical downscaling simulation and projection for mean and extreme temperature and precipitation over central Asia. *Clim. Dyn.* 54 (7–8), 3279–3306. <https://doi.org/10.1007/S00382-020-05170-0/FIGURES/17>.